EXTENDED SPECTRAL ANALYSIS OF INTERNAL QUANTUM EFFICIENCY

Paul A. Basore
Sandia National Laboratories
Albuquerque, NM 87185-5800

ABSTRACT

A powerful new method for identifying the performance-limiting mechanisms in silicon cells has been developed and tested at Sandia. This method uses the internal quantum efficiency (IQE) of the device at both near-infrared and near-bandgap wavelengths. The conventional interpretation of IQE is expanded to accommodate textured surfaces and long diffusion lengths, and extended to near-bandgap wavelengths where internal optical effects play an important role. This paper describes how the information available from this extended analysis can be used to obtain a value for the internal optical reflectance of the back surface, and to separate the effects of diffusion length from back-surface recombination. Results from experimental tests verify the method. The information obtained can be used to compute recombination components for the cell, and to quantify the light-trapping effectiveness of the device.

INTRODUCTION

The absorption coefficient for monochromatic light in silicon is a strong function of wavelength, so the spectral response of silicon solar cells contains information about their internal operation. But to study the internal operation, it is first necessary to eliminate external optical effects from the spectral response data. This can be accomplished by measuring the total hemispherical reflectance of the cell as a function of wavelength. The spectral response can be adjusted to account for the optical reflectance, yielding the internal quantum efficiency (IQE) of the device. Specifically, IQE is calculated at each wavelength from the measured spectral response, SR(λ) (amps/watt), and hemispherical reflectance, R(λ), using:

$$IQE = SR \cdot (hc/q\lambda)/(1-R), \qquad (1)$$

where λ is the free-space wavelength and hc/q = 1239.84 V·nm. IQE is intended to represent the fraction of the minority carriers photogenerated in the cell that are collected under short-circuit conditions. But, in practice, the measurement fails to accurately represent this concept because it cannot distinguish between carrier-producing absorption in the silicon and parasitic absorption. Parasitic absorption of photons at the back surface is particularly important for weakly absorbed wavelengths near the bandgap. This effect can be exploited to obtain information about the internal reflectance of the back surface [1].

The conventional interpretation of IQE data is obtained from a plot of IQE^{-1} versus α^{-1}, where the optical absorption coefficient, α, is a known function of wavelength [2]. For planar cells of thickness W with a diffusion length, L, much shorter than the thickness, the plot is linear for absorption lengths (α^{-1}) greater than the junction depth but shorter than the device thickness. The inverse of this slope is equal to the minority-carrier diffusion length in the base region.

The analysis of IQE data can be extended to accommodate textured surfaces, long diffusion lengths, and weakly absorbed light. Fig. 1 illustrates the optical model on which the method described in this paper is based. Incident light is partially reflected at the external front surface (R_{fe}). That which gets into the silicon is refracted to an angle θ_1 by the front-surface texture. For chemically textured (100)-oriented silicon, this angle is 41.8° for $\lambda \approx 900$ nm. If the energy of the photons is near the bandgap of silicon, some fraction of the light (T_1) will be transmitted to the back surface of the cell, where it will be partially reflected back toward the front of the cell (R_{b1}). If the rear surface is polished, these reflected rays will retain the same path angle on their return trip (θ_2). But if the rear surface is rough, the rays will be at least partially randomized in their return orientation. When the reflected light is completely randomized, the effective path angle is 60°. Partially randomized light will have a smaller effective path angle.

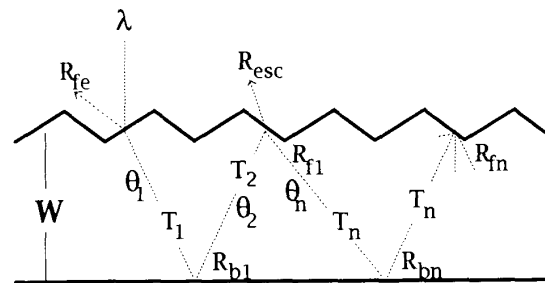
Fig. 1. Optical Model for Extended IQE Analysis.

A portion of the reflected light (T_2) will reach the internal front surface of the cell. Some of this light will escape out the front, contributing to the measured hemispherical reflectance (R_{esc}); the rest will be reflected back inside for another pass (R_{f1}). Any rays that remain trapped inside the cell at this point are probably completely random in their orientation. They will continue to bounce back and forth, with a certain transmittance

for each pass (T_n), and with successive internal reflectances at the back (R_{bn}) and front (R_{fn}) surfaces.

This paper will describe how this optical model can be used to extract information from the spectral dependence of internal quantum efficiency. Equations are presented which incorporate all of the parameters of this model. A sensitivity analysis of the model was used to identify which parameters have the greatest effect on the measured data. Only a few parameters are shown to be important, allowing data interpretation to be simplified significantly. Finally, the method is verified by evaluating cells fabricated at Sandia under controlled conditions designed to vary only one cell parameter at a time.

THE DATA

IQE data has been collected in Sandia's Photovoltaic Device Measurement Laboratory for more than a decade. Recently, the hardware used for the spectral response measurement has been significantly improved. The absolute accuracy of this system is currently estimated at better than $\pm 2\%$ for wavelengths between 400 and 1120 nm. IQE has since been measured on more than 100 cells using this new system. Plots of inverse-IQE versus absorption length for the wavelength range 800 nm to 1120 nm have consistently displayed two linear regimes, as illustrated in Fig. 2 for a textured high-performance silicon cell fabricated at Sandia.
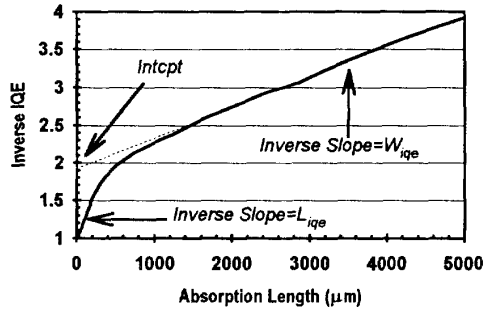

Fig. 2. Typical Inverse-IQE data showing two linear regimes.

The first linear regime occurs at near-infrared wavelengths. This is the data conventionally used to interpret IQE. But, for a textured cell such as this one, the inverse slope, L_{iqe}, cannot be directly equated to the diffusion length. The second linear regime occurs at near-bandgap wavelengths. The existence of the second linear regime was first predicted using the computer program PC-1D [4]. The inverse slope of this region, W_{iqe}, and the extrapolated intercept of this line with the axis, Intcpt, form the basis for an "extended IQE analysis."

THE EQUATIONS

The numerator of equation (1) can be expressed as the product of the fraction of the incident photons that are absorbed (f_{abs}) times the probability that the carriers generated by this absorption are successfully collected at the junction (η_c):

$$IQE = f_{abs}\eta_c / (1 - R). \qquad (2)$$

The optical model of Fig. 1 can be used to derive expressions for f_{abs} and R, while an electrical model is needed to determine an expression for η_c.

Optical Model Equations

The fraction of the incident light absorbed in the cell, excluding parasitic absorption at the back surface, is

$$f_{abs} = (1 - R_{fe})\left\{ \begin{array}{l} (1 - T_1) + R_{b1}T_1(1 - T_2) \\ + \dfrac{R_{b1}R_{f1}T_1T_2(1 - T_n)(1 + R_{bn}T_n)}{1 - R_{bn}R_{fn}T_n^2} \end{array} \right\}. \qquad (3)$$

The total reflectance, including escape reflectance, is given by

$$1 - R = (1 - R_{fe})\left\{ \begin{array}{l} 1 - R_{b1}T_1T_2(1 - R_{f1}) \\ - \dfrac{R_{b1}R_{f1}T_1T_2R_{bn}(1 - R_{fn})T_n^2}{1 - R_{bn}R_{fn}T_n^2} \end{array} \right\}. \qquad (4)$$

Electrical Model Equations

The electrical model used in this work is a simple one. The base region of the cell is a quasi-neutral region in low-level injection, characterized by a uniform minority-carrier diffusion length (L) and diffusivity (D), and a surface recombination velocity (S) at the back surface. The collecting junction is assumed to be located at the front surface. The wavelength range considered is restricted to $\lambda > 800$ nm so that the influence of recombination in the thin emitter region can be neglected.

Despite this simple model, an analytical expression valid over the entire wavelength range would be extraordinarily complex, because the photogeneration profile in the device is affected by light trapping at the longer wavelengths. However, simple expressions can be obtained in two limiting cases: (1) for near-infrared wavelengths unaffected by light trapping, and (2) at near-bandgap wavelengths where photogeneration is uniform throughout the device.

For near-infrared wavelengths, the product αW is much greater than 1, so none of the photons penetrate to the back surface. The fraction of the photogenerated carriers that are collected under short-circuit conditions, η_c, is a function of wavelength because it depends on the absorption depth of the light [3]. For a planar surface, the collection efficiency in this limit is:

$$\eta_c = \frac{\alpha L}{\alpha^2 L^2 - 1}\left\{ \alpha L - \frac{\dfrac{SL}{D} + \tanh \dfrac{W}{L}}{1 + \dfrac{SL}{D}\tanh \dfrac{W}{L}} \right\}. \qquad (5)$$

With a textured surface, the only difference is that the light traverses the cell at an angle θ_1, so that it is necessary to replace α in equation (5) with $\alpha/\cos\theta_1$. Equation (5) can be

simplified by considering its behavior for different values of L. When L<<W, the expression in brackets reduces to {αL-1}. When L is comparable to or greater than W, unity terms can be ignored compared to terms of the order $\alpha^2 L^2$, because of the initial premise that αW>>1 (hence αL>>1).

For near-bandgap wavelengths, light is absorbed slowly and photogeneration occurs uniformly throughout the device. The fraction of the generated carriers that are collected under short-circuit conditions, η_c, becomes independent of wavelength [4]:

$$\eta_c = \frac{L}{W} \cdot \frac{\frac{SL}{D} + \tanh\frac{W}{L} - \frac{SL/D}{\cosh\frac{W}{L}}}{1 + \frac{SL}{D}\tanh\frac{W}{L}}. \tag{6}$$

IQE Equation for Near-Infrared Wavelengths

For wavelengths that do not penetrate to the rear surface, equation (3) gives the expected result that f_{abs}=1-R_{fe}. In silicon, the range of wavelength where this limit applies is approximately 800 nm to 1000 nm. Incorporating the simplifications mentioned for equation (5), a single expression for inverse-IQE at near-infrared wavelengths can be written that is valid for all values of L:

$$IQE^{-1} = 1 + \frac{\cos\theta_1}{\alpha L_{eff}}, \tag{7}$$

where

$$L_{eff} = L \cdot \frac{1 + \frac{SL}{D}\tanh\frac{W}{L}}{\frac{SL}{D} + \tanh\frac{W}{L}}. \tag{8}$$

Equation (7) predicts a linear dependence of inverse-IQE on absorption length, just as in the conventional interpretation of IQE, but with inverse slope $L_{iqe}=L_{eff}/\cos\theta_1$ in place of L. It is quite useful to note that L_{eff} as defined in equation (8) is the same effective diffusion length that determines the base component of the dark saturation current density:

$$J_{ob} = \frac{qDn_i^2}{N_B L_{eff}}, \tag{9}$$

where N_B is the base doping density and n_i is the intrinsic carrier concentration (n_i=8.6x10^9 cm^{-3} for Si at 25°C).

IQE Equation for Near-Bandgap Wavelengths

For wavelengths that are only weakly absorbed, the wavelength dependence of IQE derives not from the electrical collection efficiency, but rather from the optical absorptance. The expressions for f_{abs} and 1-R given in equations (3) and (4) can be inserted into the expression for IQE given in equation (2) to obtain the following rather complicated expression for inverse IQE in the near-bandgap wavelength range:

$$IQE^{-1} = \frac{1}{\eta_c} \cdot \frac{\begin{array}{c}[1 - R_{b1}T_1T_2(1-R_{f1})][1 - R_{bn}R_{fn}T_n^2] \\ -R_{b1}R_{f1}T_1T_2R_{bn}(1-R_{fn})T_n^2\end{array}}{\begin{array}{c}[(1-T_1) + R_{b1}T_1(1-T_2)][1 - R_{bn}R_{fn}T_n^2] \\ +R_{b1}R_{f1}T_1T_2(1-T_n)(1+R_{bn}T_n)\end{array}}. \tag{10}$$

In silicon, the wavelength range over which this expression is appropriate is approximately 1080 nm to 1120 nm. At shorter wavelengths the absorption is not spatially uniform. At longer wavelengths the absorption coefficient is too uncertain, being affected by free-carrier absorption and temperature-induced variation in the bandgap.

The dominant wavelength dependence of equation (10) lies in the transmittances T_1, T_2, and T_n, where

$$T_1 = e^{-\alpha W/\cos\theta_1}, \quad T_2 = e^{-\alpha W/\cos\theta_2}, \quad T_n = e^{-\alpha W/\cos\theta_n}. \tag{11}$$

For weakly absorbed light, the transmittances in equation (11) can be expressed as an infinite series involving powers of α. The numerator and denominator of equation (10) can, in turn, be expressed as two power series involving α:

$$IQE^{-1} = \frac{1}{\eta_c} \cdot \frac{a_0 + a_1(\alpha W) + a_2(\alpha W)^2 + ...}{b_0 + b_1(\alpha W) + b_2(\alpha W)^2 + ...}, \tag{12}$$

The denominator term b_0 is equal to zero; so that, for small α, the two largest terms in the expression for IQE^{-1} are of the order α^{-1} and α^0. This corresponds to the anticipated linear dependence of inverse-IQE on inverse absorption coefficient:

$$IQE^{-1} \cong \frac{1}{\eta_c} \cdot \left\{ \frac{a_1 b_1 - a_0 b_2}{b_1^2} + \frac{a_0}{b_1}(\alpha W)^{-1} \right\}, \tag{13}$$

where

$a_0 = [1 - R_{b1}(1-R_{f1})][1 - R_{bn}R_{fn}] - R_{b1}R_{bn}R_{f1}(1-R_{fn}),$

$a_1 = R_{b1}[1 - R_{f1} - R_{bn}(R_{fn} - R_{f1})][\frac{1}{\cos\theta_1} + \frac{1}{\cos\theta_2}]$
$\quad + 2[R_{fn} - R_{b1}(R_{fn} - R_{f1})][\frac{R_{bn}}{\cos\theta_n}],$

$b_1 = [\frac{1}{\cos\theta_1} + \frac{R_{b1}}{\cos\theta_2}][1 - R_{bn}R_{fn}] + R_{b1}R_{f1}\frac{(1+R_{bn})}{\cos\theta_n},$

$b_2 = \frac{2R_{bn}R_{fn}}{(\cos\theta_1\cos\theta_n)} - \frac{0.5(1-R_{bn}R_{fn})}{\cos^2\theta_1}$
$\quad + \frac{2R_{b1}R_{bn}R_{fn}}{(\cos\theta_2\cos\theta_n)} - \frac{R_{b1}(1-R_{bn}R_{fn})}{(\cos\theta_1\cos\theta_2)}$
$\quad - \frac{0.5R_{b1}(1-R_{bn}R_{fn})}{\cos^2\theta_2} - \frac{R_{b1}R_{f1}R_{bn}}{\cos^2\theta_n}$
$\quad - R_{b1}R_{f1}(1+R_{bn})[\frac{1}{(\cos\theta_1\cos\theta_n)} + \frac{1}{(\cos\theta_2\cos\theta_n)}]$
$\quad - \frac{0.5R_{b1}R_{f1}(1+R_{bn})}{\cos^2\theta_n}.$

From the linear dependence of IQE^{-1} on α^{-1} demonstrated in equation (13), the expressions for W_{iqe} and Intcpt are:

$$W_{iqe} = \eta_c W \frac{b_1}{a_0},$$ (14)

$$Intcpt = \frac{1}{\eta_c} \cdot \frac{a_1 b_1 - a_0 b_2}{b_1^2}.$$

Note that the product $W_{iqe} \cdot$Intcpt eliminates η_c. This product depends only on the optical properties of the cell, and is independent of the cell's electrical properties!

Auxiliary Optical Definitions

Two commonly encountered parameters when discussing light trapping in silicon cells are the light-trapping effectiveness factor, Z [5], and the sub-bandgap reflectance, R_{sub}. The optical model presented in this paper can be used to derive analytical expressions for these two quantities.

The Z factor for near-bandgap wavelengths is defined here as a thickness multiplier for uniformly absorbed wavelengths:

$$Z = \frac{\lim_{\alpha \to 0} f_{abs}}{(1 - R_{fe})\alpha W} = \frac{b_1}{1 - R_{bn} R_{fn}},$$ (15)

where b_1 is from equation (13). The sub-bandgap reflectance is from equation (4), by setting $T_1 = T_2 = T_n = 1$:

$$1 - R_{sub} = \frac{(1 - R_{fe})a_0}{1 - R_{bn} R_{fn}},$$ (16)

where a_0 is also from equation (13). Note that

$$Z = \frac{b_1}{a_0} \cdot \frac{(1 - R_{sub})}{(1 - R_{fe})} = \frac{W_{iqe}}{\eta_c W} \cdot \frac{(1 - R_{sub})}{(1 - R_{fe})}.$$ (17)

SENSITIVITY ANALYSIS

The value of $W_{iqe} \cdot$Intcpt depends only on the optical parameters of the cell. But the optical model for near-bandgap wavelengths involves far more parameters than can be found using IQE data alone. A sensitivity analysis was performed to determine which optical parameters have the greatest effect on $W_{iqe} \cdot$Intcpt. This analysis was performed for several different types of cells. The results of the analysis are shown in Table I for a textured cell, and in Table II for a cell with a planar front surface but a rough rear surface. The values of the optical parameters used to describe each cell are listed in the tables.

The topology of the cell provides, by itself, some information about the optical parameters. This *a priori* knowledge is listed in the tables as the pre-data uncertainty for each parameter. The effect of each optical parameter on the dimensionless factor $W_{iqe} \cdot$Intcpt/W was calculated and is expressed in the tables as

TABLE I
SENSITIVITY ANALYSIS: TEXTURED CELL
$R_{fl} = .7,\ R_{fn} = .92, R_{bl} = .7, R_{bn} = .7, \cos\theta_1 = .75, \cos\theta_2 = .65, \cos\theta_n = .5$

Optical Parameter		$W_{iqe} \cdot$Intcpt/W		Post-Data
Symbol	Pre-Data Uncertainty	Sensitivity Factor	Pre-Data Uncertainty	Parameter Uncertainty
R_{fl}	25%	+0.06	2%	25%‡
R_{fn}	5%	+0.25	1%	5%
R_{bl}	30% (5%)†	+0.45	14%	5%
R_{bn}	30%	**+2.51**	**75%**	3%
$\cos\theta_1$	10%	-0.03	0%	10%
$\cos\theta_2$	20%	-0.07	1%	20%
$\cos\theta_n$	5%	-0.89	4%	5%

†Because $R_{bl} \approx R_{bn}$, the smaller value applies if R_{bn} is known.
‡The uncertainty in R_{fl} can be reduced to 13% by measuring the sub-bandgap reflectance and using equation (16).

TABLE II
SENSITIVITY ANALYSIS: PLANAR CELL
$R_{fl} = .6,\ R_{fn} = .92, R_{bl} = .7, R_{bn} = .7, \cos\theta_1 = 1, \cos\theta_2 = .75, \cos\theta_n = .5$

Optical Parameter		$W_{iqe} \cdot$Intcpt/W		Post-Data
Symbol	Pre-Data Uncertainty	Sensitivity Factor	Pre-Data Uncertainty	Parameter Uncertainty
R_{fl}	50%	+0.09	4%	50%‡
R_{fn}	10%	+0.41	4%	10%
R_{bl}	30% (5%)†	+0.47	14%	5%
R_{bn}	30%	**+2.53**	**76%**	5%
$\cos\theta_1$	5%	-0.01	0%	5%
$\cos\theta_2$	30%	-0.07	2%	30%
$\cos\theta_n$	10%	-0.90	9%	10%

†Because $R_{bl} \approx R_{bn}$, the smaller value applies if R_{bn} is known.
‡The uncertainty in R_{fl} can be reduced to 20% by measuring the sub-bandgap reflectance and using equation (16).

a sensitivity coefficient — the percent change in the factor for a 1% change in the corresponding optical parameter. The pre-data uncertainty listed in the tables for $W_{iqe} \cdot$Intcpt/W is just the product of the pre-data uncertainty in each parameter times the sensitivity of $W_{iqe} \cdot$Intcpt/W to that parameter. This indicates how much additional uncertainty would be introduced if the *a priori* value of that parameter was assumed in the model. From this column it is quite clear that for both types of cells illustrated, the factor $W_{iqe} \cdot$Intcpt/W is completely dominated by R_{bn}. Even if inaccurate *a priori* assumptions are made for all other optical parameters, it is still possible to

determine an accurate value for R_{bn} directly from the measured value of $W_{iqe}\cdot Intcpt/W$. The dependence of this factor on R_{bn} is shown in Fig. 3 for the two types of cells considered.
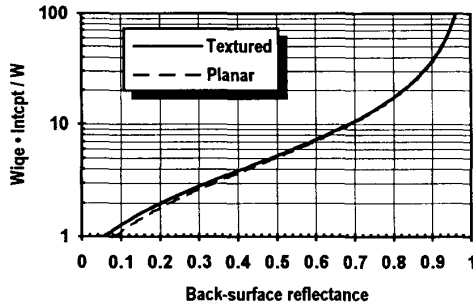

Fig. 3. Graphical representation showing how R_{bn} can be determined directly from the measured value of $W_{iqe}\cdot Intcpt/W$.

The value obtained for R_{bn} using Fig. 3 has an estimated uncertainty of 5% or less, as listed in the tables. This estimate is obtained by assuming that $W_{iqe}\cdot Intcpt/W$ has its own measurement uncertainty of 5%, which is increased (using root-sum-squares) by the uncertainties in $W_{iqe}\cdot Intcpt/W$ due to having assumed values for all of the optical parameters other than R_{bn}. This total uncertainty in $W_{iqe}\cdot Intcpt/W$, approximately 10%, is divided by the model's sensitivity to R_{bn} to obtain the post-data uncertainty listed in the table for R_{bn}.

A similar sensitivity analysis was conducted for the electrical collection efficiency, η_c. The collection efficiency is approximately equal to $1/Intcpt$, with some influence from the parameters R_{b1} and R_{bn}. Since usually $R_{b1}\approx R_{bn}$, and R_{bn} is known to within 5% from Fig. 3, it is possible to determine η_c with similar accuracy: ±4% for the textured cell and ±8% for the planar cell. Fig. 4 illustrates the dependence of the product $\eta_c\cdot Intcpt$ on the back-surface reflectance.

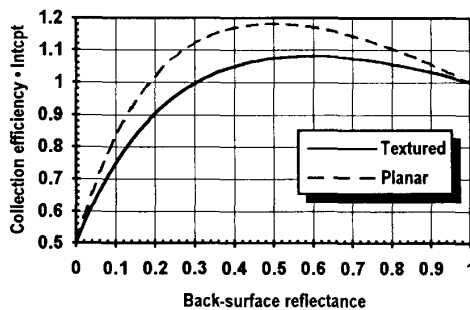Fig. 4. Graphical representation showing how R_b and Intcpt can be used to determine η_c, for two different cell types.

The model presented here does not consider parasitic optical absorption other than at the back surface. If a cell with parasitic

absorption at the front surface is evaluated using this model, the effect will be an apparent reduction in the value of R_{bn}.

SEPARATING THE EFFECT OF S FROM L

The relative significance of bulk recombination versus back-surface recombination can be evaluated by combining the results from the near-infrared wavelengths with results from the near-bandgap analysis. L_{eff}/W provides one relationship between the dimensionless electrical parameters L/W and SW/D. The collection efficiency, η_c, provides a different relationship between L/W and SW/D. In principle, equations (6) and (8) can be solved together to obtain both L and S. But not every combination of L_{eff}/W and η_c is physically possible. This constraint is clarified by Fig. 5, in which the cross-hatched area shows the parameter space that can satisfy both equations.
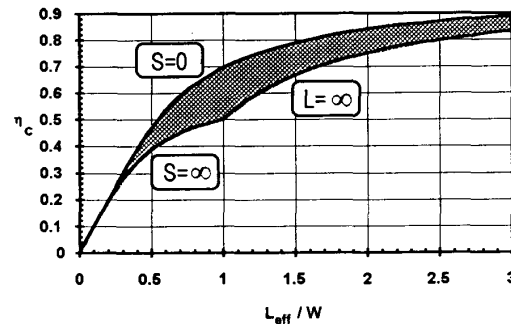

Fig. 5. Range of possible combinations of L_{eff}/W and η_c. No finite combination of L and S yields results outside this range.

In the lower-left corner of the parameter space shown in Fig. 5, $L<<W$. Here L dominates and can be found accurately, but no information is available regarding S. In the upper-right corner, recombination in the bulk and at the back surface are both small. The upper curve represents bulk-dominated recombination, while the lower curve represents surface-dominated recombination. In this region, the uncertainty inherent in η_c makes it possible only to determine whether one recombination mechanism is dominant, and if so which one. In the cross-hatched area near the center of the figure, the two equations can be solved to obtain meaningful values for both L and S, with greater accuracy for the dominant factor.

EXPERIMENTAL VERIFICATION

Extended IQE analysis has been applied to a wide variety of silicon cells over the past year, using spectral response and reflectance data from Sandia's Photovoltaic Device Measurement Laboratory. The method has been particularly useful for characterizing high-performance cells which combine long diffusion lengths with light trapping.

The most comprehensive tests of the method have been performed on cells prepared in Sandia's Photovoltaic Device Fabrication Laboratory under carefully controlled conditions. One test involved the coprocessing of cells with and without

151

TABLE III
Experimental Comparison of Planar versus Textured Front Surface
PDFL Lot BL1-10   Wafers: 10 Ωcm p-type Si, W=640 µm, Aluminum Rear

Surface	$L_{iqe}(\mu m)$	$L_{eff}(\mu m)$	$W_{iqe}(\mu m)$	Intcpt	R_{bn}	η_c
Planar	260	260	2370	2.50	66%	43%
Textured	345	260	2300	2.45	65%	44%

TABLE IV
Experimental Comparison of Back-Surface Metals
PDFL Lot BL1-11   Wafers: 2 Ωcm p-type Si, W=460 µm, Textured

Rear Metal	$L_{iqe}(\mu m)$	$L_{eff}(\mu m)$	$W_{iqe}(\mu m)$	Intcpt	R_{bn}	η_c
Aluminum	273	205	1930	2.23	67%	48%
Titanium	256	192	390	1.50	9%	48%

TABLE V
Experimental Evaluation of Al BSF on Different Wafer Materials
PDFL Lot BL1-21   Wafers: p-type Si, Textured, Aluminum-Alloy Rear

Material	$W(\mu m)$	$L_{eff}(\mu m)$	$W_{iqe}(\mu m)$	Intcpt	R_{bn}	η_c	$L(\mu m)$	$S(cm/s)$
2 Ωcm	470	380	2780	1.80	69%	60%	350	400
10 Ωcm	585	600	3760	1.61	69%	67%	540	200

chemical front-surface texturing. Both cell types received the same back-surface aluminum evaporation. Despite substantial differences in spectral response and reflectance for these two cells, the internal parameters deduced are nearly identical, as listed in Table III. In a second test, textured cells were identically prepared except that the back metal was either aluminum or titanium. According to the analysis, only the back reflectance was significantly affected, as shown in Table IV. A third test was performed which subjected two different wafer materials to identical processing. Table V lists the parameters that were extracted from these cells, including estimates of L and S. Both materials received the same aluminum-alloy back-surface treatment, and the analysis reveals nearly identical back-surface reflectance, despite significant differences in diffusion length and wafer thickness.

CONCLUSIONS

Analysis of internal quantum efficiency data has been extended for near-infrared wavelengths to accommodate textured cells and long diffusion lengths. The slope of the inverse IQE plot in this wavelength range gives the effective diffusion length needed to calculate the base component of the saturation current density to within about 5%. If the total saturation current density is known from dark I-V or I_{sc}-V_{oc} data, one can assess the relative importance of the base versus the emitter in determining the cell's voltage.

The additional information available from near-bandgap wavelengths permits the determination of the internal back-surface reflectance and the carrier collection efficiency for uniform photogeneration, to within about 5%. By combining the effective diffusion length from the near-infrared wavelengths with the collection efficiency from the near-bandgap wavelengths, it is possible to identify whether the dominant recomination mechanism in the base region of the cell is in the bulk or at the back surface.

Our experience at Sandia over the past year indicates that the extended-IQE analysis described here is the most reliable method yet devised for identifying the performance-limiting mechanisms in silicon solar cells, especially those which combine long diffusion lengths and light trapping. Most importantly, IQE analysis is performed nondestructively, on finished cells, using data that directly reflects the cell's performance.

REFERENCES

[1] James M. Gee, "The Effect of Parasitic Absorption Losses on Light Trapping in Thin Silicon Solar Cells," *20th IEEE PVSC* (September 1988), p. 549.

[2] Martin A. Green, *High Efficiency Silicon Solar Cells*, Trans Tech Publications, Switzerland, 1987, Appendix C.

[3] S.M. Sze, *Physics of Semiconductor Devices*, 2nd Ed., John Wiley & Sons, New York, 1981, p. 803.

[4] Paul A. Basore, "Numerical Modeling of Textured Silicon Solar Cells Using PC-1D," *IEEE Trans. on Electron Devices*, ED-37 (February 1990), p. 337.

[5] James A. Rand and Paul A. Basore, "Light-Trapping Silicon Solar Cells: Experimental Results and Analysis," *22nd IEEE PVSC* (October 1991), p. 192.